

PROJECTED ROTATIONAL VELOCITIES AND STELLAR CHARACTERIZATION OF 350 B STARS IN THE NEARBY GALACTIC DISK

G. A. BRAGANÇA¹, S. DAFLON¹, K. CUNHA^{1,2,3}, T. BENSBY⁴, M. S. OEY⁵, AND G. WALTH⁶

¹ Observatório Nacional-MCT, Rua José Cristino, 77, CEP 20921-400, Rio de Janeiro-RJ, Brazil; braganca@on.br

² National Optical Astronomy Observatory, 950 North Cherry Avenue, Tucson, AZ 85719, USA

³ Department of Astronomy/Steward Observatory, University of Arizona, 933 North Cherry Ave., Rm. N204, Tucson, AZ 85721-0065, USA

⁴ Lund Observatory, Department of Astronomy and Theoretical Physics, Box 43, SE-22100, Lund, Sweden

⁵ Astronomy Department, University of Michigan, 830 Dennison Building, Ann Arbor, MI 48109-1042, USA

⁶ Steward Observatory, University of Arizona, 933 North Cherry Avenue, Tucson, AZ 85721, USA

Received 2012 April 27; accepted 2012 August 1; published 2012 September 28

ABSTRACT

Projected rotational velocities ($v \sin i$) are presented for a sample of 350 early B-type main-sequence stars in the nearby Galactic disk. The stars are located within ~ 1.5 kpc from the Sun, and the great majority within 700 pc. The analysis is based on high-resolution spectra obtained with the MIKE spectrograph on the Magellan Clay 6.5 m telescope at the Las Campanas Observatory in Chile. Spectral types were estimated based on relative intensities of some key line absorption ratios and comparisons to synthetic spectra. Effective temperatures were estimated from the reddening-free Q index, and projected rotational velocities were then determined via interpolation on a published grid that correlates the synthetic FWHM of the He I lines at 4026, 4388 and 4471 Å with $v \sin i$. As the sample has been selected solely on the basis of spectral types, it contains a selection of B stars in the field, in clusters, and in OB associations. The $v \sin i$ distribution obtained for the entire sample is found to be essentially flat for $v \sin i$ values between 0 and 150 km s⁻¹, with only a modest peak at low projected rotational velocities. Considering subsamples of stars, there appears to be a gradation in the $v \sin i$ distribution with the field stars presenting a larger fraction of the slow rotators and the cluster stars distribution showing an excess of stars with $v \sin i$ between 70 and 130 km s⁻¹. Furthermore, for a subsample of potential runaway stars we find that the $v \sin i$ distribution resembles the distribution seen in denser environments, which could suggest that these runaway stars have been subject to dynamical ejection mechanisms.

Key words: stars: early-type – stars: fundamental parameters – stars: rotation

Online-only material: color figures, machine-readable and VO tables

1. INTRODUCTION

O- and B-type stars, with typical values of projected rotational velocities ($v \sin i$) around 100 km s⁻¹ and higher, have the largest average $v \sin i$ values among all main-sequence stars. Stellar rotation appears to be a fundamental parameter constraining the formation of these massive stars and the environments in which they are born, as well as their subsequent evolution. For instance, there is observational evidence that stars formed in denser environments tend to rotate faster than those formed in associations (Wolff et al. 2007) and for O and B stars in the field the proportion of slow rotators seems to be even higher (see Huang & Gies 2006 for open clusters and Daflon et al. 2007 for the Cep OB2 association). In addition, rotation may modulate the formation of massive field stars. Oey & Lamb (2011) cite this trend, together with additional empirical evidence based on the stellar clustering law, initial mass function, and direct observations, as evidence that significant numbers of field massive stars form in situ, i.e., they were not born in clusters. Also, rotation might help in understanding the origin of runaway stars. $v \sin i$ distributions of runaway stars have not been studied much in the literature. Martin (2006) studied the $v \sin i$ distribution of high latitude OB runaway stars and noted the lack of slow rotators compared to a field sample. This was interpreted in that study as evidence that those runaway stars might have been ejected from OB associations.

The study of $v \sin i$ distributions of samples of OB stars born in different environments, such as clusters, OB associations, or the general Galactic field, and selected without bias concerning

cluster membership, can be used to probe the interplay between star formation and stellar rotation. In this paper, we analyze such a sample; we present the spectroscopic observations and a first characterization of a sample of 350 OB stars located within ~ 2 kpc from the Sun. The goal of this study is to define the stars in terms of their effective temperatures, along with their projected rotational velocities, with the emphasis on the $v \sin i$ distributions from stars in different environments. These stars will be analyzed in terms of their chemical composition in a future study. This paper is divided as follows: Section 2 describes the observations and sample selection; Section 3.1 selects from the observed sample the binary or multiple stars; Section 3.2 discusses the derived effective temperatures and spectral classification for the sample. Finally, projected rotational velocities are derived in Section 4. In Section 5, we discuss the $v \sin i$ distributions obtained for the studied sample and in Section 6, we present the conclusions.

2. OBSERVATIONS AND THE SAMPLE

Based on the spectral type as the sole criterion, we selected 379 O9 to B4 main-sequence stars from the *Hipparcos* catalog (Perryman et al. 1997). High-resolution spectra were then obtained for these stars on 2007 January 8, 9 and April 8 with the MIKE spectrograph at the Magellan Clay 6.5 m telescope on Las Campanas observatory in Chile. MIKE (Bernstein et al. 2003) is a double échelle spectrograph that registers the whole spectrum on two CCDs (red side 4900–9500 Å and blue side 3350–5000 Å) in a single exposure. Here, the blue spectra are

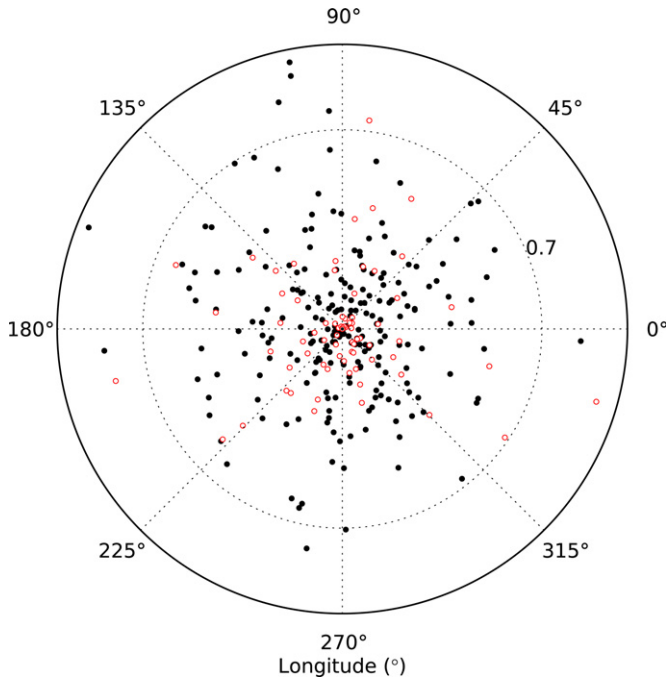


Figure 1. Polar plot showing the positions of the sample stars projected onto the Galactic plane. The radius is limited to 1 kpc and the concentric dotted circle represents the distance of 0.7 kpc, within which $\sim 80\%$ of the stars in our sample are located. The open red circles are spectroscopic binaries/multiple systems identified in our sample. Values for distance of the stars are more uncertain beyond 0.5 kpc of the Sun.

(A color version of this figure is available in the online journal.)

analyzed as these contain most of the diagnostic spectral lines needed for estimating $v \sin i$, spectral type, and the effective temperature (T_{eff}) of the star. The spectral resolution of the observed spectra is $R \sim 55,000$ and was obtained using a slit width of 0.7 arcsec.

In order to minimize possible evolutionary effects on the $v \sin i$ and given that the He I line width calibration adopted in this study (Daffon et al. 2007, Section 4) is valid for main-sequence stars, we screened the observed spectra in order to exclude all evolved stars from the sample. The Balmer lines and other spectral features which are sensitive to surface gravity such as, the line ratios $\lambda 4686 \text{ He II} / \lambda 4713 \text{ He II}$ (stars with spectral types O9–B0) and $\lambda 4552 \text{ Si III} / \lambda 4387 \text{ He I}$ (stars classified as B1 or later), were used as the primary luminosity criteria. Our final sample consists of 350 stars and is expected to contain only main-sequence stars and not giants or supergiants.

The observed sample of stars is displayed in Figure 1 in terms of their Galactic longitude and heliocentric distance projected onto the Galactic plane. The stars in the sample are all nearby ($\sim 80\%$ is within 700 pc) and relatively bright ($V \sim 5\text{--}10$). Spectra with signal-to-noise ratios of the order of 100 were achieved with short exposure times ranging from a few seconds to a few minutes. The spectra were reduced with the Carnegie Observatories python pipeline⁷ and followed standard data reduction procedures: bias subtraction, division by flat field, and wavelength calibration. In addition, small pieces containing the lines of interest were manually normalized to a unit continuum using the task `continuum` in IRAF.⁸ Sample spectra are shown in Figure 2 in the spectral region between 4625 and 4665 Å, which contains spectral lines of C, N, O, and Si. The spectra are

Table 1
Binary/multiple Stars

HIP	Spectral Type	Bin.
17563	B3V	Lef09, ET08
17771	B3V	ET08
21575	B3V	SB, Lef09
22663	B2/B3V	Asym., Lef09
25028	B3V	SB, ET08

Notes. The columns are: (1) the *Hipparcos* identification, (2) the spectral type, (3) Binarity/multiplicity: we classified the star as “asym.” when it has an asymmetric line profile or “SB” when it is a spectroscopic binary. Some stars are listed as binaries in Lefèvre et al. (2009, Lef09) and/or Eggleton & Tokovinin (2008, ET08).

(This table is available in its entirety in machine-readable and Virtual Observatory (VO) forms in the online journal. A portion is shown here for guidance regarding its form and content.)

shown for five target stars and these are displayed in order of increasing temperature.

3. STELLAR CHARACTERIZATION

3.1. Identification of Spectroscopic Binaries

It is likely that most massive OB stars form in clusters or associations, with the probability of a star forming with a companion being high. The recent study by Oudmaijer & Parr (2010), for example, found a binary fraction of $\sim 30\%$ in their photometric survey of B and Be stars. A first objective in this study is to identify those stars, among the 350 stars observed, that show spectral signatures of binary or multiple components. This was done through a careful visual inspection of their spectra. Single-line spectroscopic binaries are not detected here, as the spectra are only from single epoch observations. Spectroscopic binaries will be discarded from further analysis in this study since the methodology here is most appropriate for spectra showing a single component.

Some stars in our sample were identified as clearly having double, multiple, or asymmetric spectral lines. In addition, some stars in our sample which were found to be binary or multiple systems in the large survey of stellar multiplicity within the *Hipparcos* catalog by Eggleton & Tokovinin (2008) and/or appeared as binaries in the study of OB star variability based on *Hipparcos* photometry by Lefèvre et al. (2009). Table 1 lists 78 stars culled from the sample as spectroscopic binaries or multiple systems, representing 22% of the stars in our sample. Column 1 has the star identification, Column 2 lists the spectral types from SIMBAD.⁹ In Column 3, stars are classified as “SB,” if they were found here to be a spectroscopic binary or multiple system; “asym.” if they exhibited asymmetric line profiles; and ET08 and Lef09 if they were in Eggleton & Tokovinin (2008) or Lefèvre et al. (2009). The stars in Table 1 will not be analyzed in the remainder of this paper.

3.2. Spectral Types and Effective Temperatures

The spectral types of the stars were determined based on the classification system presented in the Atlas of OB stars by Walborn & Fitzpatrick (1990). Relative intensities of some key absorption line ratios such as: $\lambda 4471 \text{ He I} / \lambda 4481 \text{ Mg II}$; $\lambda 4630 \text{ N II} / \lambda 4631 \text{ Si IV}$; $\lambda 4641 \text{ N III} / \lambda 4643 \text{ N II}$, and $\lambda 4649$

⁷ Available at <http://obs.carnegiescience.edu/Code/mike>.

⁸ <http://iraf.noao.edu/>

⁹ <http://simbad.u-strasbg.fr>

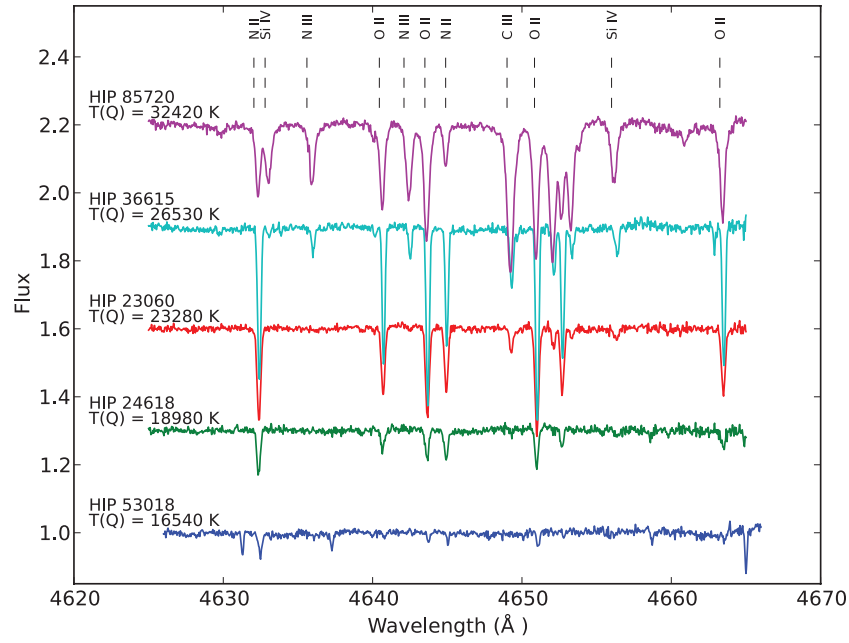


Figure 2. Example spectra of five sample stars in the region 4625–4665 Å. Some spectral lines are identified. The spectra were arbitrarily displaced in intensity for better viewing.

(A color version of this figure is available in the online journal.)

Table 2
v sin i Results for the Entire Sample

HIP	Spectral Type	V	Q	T_{eff} (K)	FWHM (Å)			$v \sin i$ (km s $^{-1}$)			$\langle v \sin i \rangle$ (km s $^{-1}$)	$\sigma(v \sin i)$ (km s $^{-1}$)	N	Memb.
					(4026 Å)	(4388 Å)	(4471 Å)	(4026 Å)	(4388 Å)	(4471 Å)				
(1)	(2)	(3)	(4)	(5)	(6)	(7)	(8)	(9)	(10)	(11)	(12)	(13)	(14)	(15)
14898	B5V	7.03	-0.41	14610	...	1.0	0.7	...	5	4	4	1	2	R
15188	B3Ve	7.96	-0.53	17290	4.2	3.9	3.7	153	151	118	141	19	3	R
16466	B4V	9.32	-0.51	16780	1.7	1.5	1.0	22	30	...	26	5	2	R
18926	B3V	6.45	-0.62	19930	5.7	5.7	5.4	234	235	194	221	23	3	...
18957	B3V	5.31	-0.5	16540	1.8	1.6	1.2	28	33	23	28	5	3	...

Notes. The columns are: (1) *Hipparcos* identification; (2) spectral type; (3) apparent magnitude V ; (4) value of the Q parameter; (5) effective temperature T_{eff} ; (6, 7, 8) FWHM in Å of the three He I lines (4026, 4388, and 4471 Å); (9, 10, 11) $v \sin i$ of the same He I lines; (12) mean $v \sin i$; (13) standard deviation of the $v \sin i$ between the available measures; (14) the number of He I lines used; and (15) the membership classification (“A” for associations, “C” for clusters, and “R” for runaway stars). All the velocities are in km s $^{-1}$.

(This table is available in its entirety in machine-readable and Virtual Observatory (VO) forms in the online journal. A portion is shown here for guidance regarding its form and content.)

C III/λ4650 O I were used to assign spectral types. In order to map the Walborn & Fitzpatrick spectral types into our sample, a small grid of non-LTE synthetic spectra of two spectral regions, 4450–4490 Å and 4630–4700 Å were computed for T_{eff} values between 15,000–33,000 K, logarithmic of the surface gravity $\log g = 4.0$, and solar composition. The theoretical spectra were calculated with the codes TLUSTY and SYNPL0T (Hubeny 1988; Hubeny & Lanz 1995). The Walborn & Fitzpatrick standard star spectra were then visually matched to their closest synthetic counterpart in the grid; spectral types assigned as O9, B0, B1, B2, B3, B4, and B5 were found to correspond to model spectra with T_{eff} values of 33,000 K, 30,000 K, 25,000 K, 20,000 K, 18,000 K, 16,000 K, and 15,000 K, respectively.

Synthetic and observed spectra were then compared by visual inspection in order to assign spectral types for the target stars. The goal was simply to determine an appropriate spectral type to each star, and not to match in detail the observed and theoretical spectra in a fine analysis. Since a fraction of the stars in our sample have spectral lines somewhat blended by

rotation, synthetic spectra were convolved for $v \sin i$ (in steps of $v \sin i = 50 \text{ km s}^{-1}$) in order to aid in the assignment of spectral types of broad-lined stars. Spectral types for the target stars are listed in Table 2 (Column 2).

Effective temperatures for the stars were estimated from a calibration of the classical reddening free parameter Q (Johnson 1958; $Q = (U - B) - X \cdot (B - V)$, where $X = E(U - B)/E(B - V)$). In order to estimate T_{eff} for the sample stars in this study, we will adopt the $T(Q)$ calibration presented in Massey et al. (1989) and defined below:

$$\log T_{\text{eff}} = 3.994 - 0.267 \cdot Q + 0.364 \cdot Q^2. \quad (1)$$

A $T(Q)$ calibration has also been proposed by Daflon et al. (1999). However, a large number of stars in the sample studied here are much cooler than the validity range of the Daflon et al. calibration. Figure 3 shows as a solid blue line the calibration by Massey et al. (1989) for the Q -interval of the stars in this study. The calibration by Daflon et al. (1999) is also

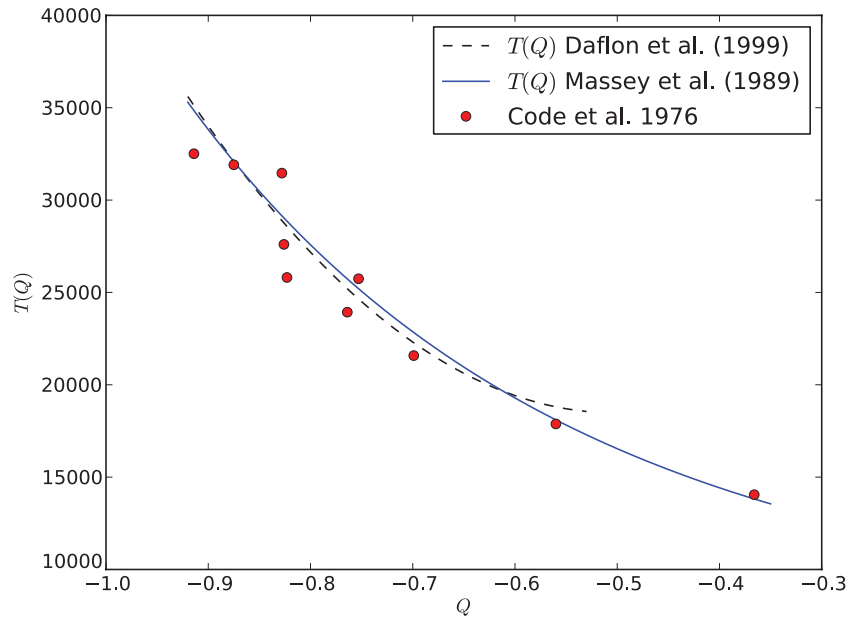


Figure 3. $T(Q)$ calibration from Massey et al. (1989, solid blue line) which was adopted in this study to estimate effective temperatures for the target stars. The Q -index calibration from Daflon et al. (1999) is also shown for comparison (black dashed line). The red filled circles represent the stars with measured radius and effective temperatures in Code et al. (1976).

(A color version of this figure is available in the online journal.)

shown in Figure 3 as black dashed line, for comparison. The average differences between the two calibrations are relatively small: $\langle \Delta T_{\text{eff}} \rangle = -380$ K and $\sigma = 177$ K, for Q -values ranging between -0.62 and -0.87 ; and $\langle \Delta T_{\text{eff}} \rangle = +583$ K and $\sigma = 405$ K for Q -values between -0.61 and -0.53 . Effective temperatures for those stars with measured radius from Code et al. (1976) are shown by red circles in Figure 3. The overall agreement of the Code et al. (1976) results with the calibrations is generally good but with significant scatter, which is indicative of the uncertainties when using the Q -index as a temperature indicator. More recently, Pauzen et al. (2005) also presented a calibration for the Q -index with the effective temperature and the $T \times Q$ relation in that study is quite similar to the one derived in Massey et al. (1989).

The Johnson color indices ($U - B$) and ($B - V$) for the studied stars were obtained from Mermilliod (1987). For those 57 stars in the sample without published Johnson photometry, UBV colors were computed from Strömgren photometry from Hauck & Mermilliod (1980, 1998), using the transformation in Harmanec & Božić (2001). In addition, there were 41 remaining stars in our sample for which there was no available photometry in the literature, and in those cases we relied on spectral types in order to obtain the intrinsic colors from the tables in Fitzgerald (1970) and then estimate Q . In Columns 3, 4, and 5 of Table 2 we list the V magnitudes, the Q parameters, and the derived T_{eff} values for 272 stars of the observed sample. The estimated T_{eff} values here are good for the purpose of a rough stellar characterization of our sample and, in particular, these suffice for a solid derivation of $v \sin i$ values since the grid of synthetic spectra used here (Section 4) has been computed for steps of 5000 K in T_{eff} .

4. PROJECTED ROTATIONAL VELOCITIES

Projected rotational velocities for the targets were estimated from measurements of the FWHM of three He I lines at 4026 Å, 4388 Å, and 4471 Å. The FWHMs of the He I line

profiles were measured using the IRAF package `splot`, using a procedure consistent with that adopted in Daflon et al. (2007): the continuum level was marked at the line center, and the half-width of the red wing was measured at the half-maximum and then doubled in order to derive the FWHM. Figure 4 shows examples of the sample He I lines for the observed stars HIP 73624 (black continuous line) and HIP 33492 (red dashed line).

The measured FWHM was converted to $v \sin i$ via interpolating in the grid of synthetic FWHM of He I lines presented in Table 2 of Daflon et al. (2007) for the adopted effective temperature of each star. The synthetic He I profiles in that study were computed in non-LTE using the codes DETAIL (Giddings 1981) and SURFACE (Butler & Giddings 1985) and were based on the helium model atom described in Przybilla (2005). We note that the macroturbulent velocity was kept as zero in the calculation of the synthetic profiles by Daflon et al. (2007) but it is likely to result in additional broadening of the line profiles. Simón-Díaz et al. (2010) did a careful analysis and disentangled the effects of macroturbulence and rotation in line profiles by using Fourier Transform method and obtained macroturbulent velocities for early B-type dwarfs that are generally lower than 20 km s^{-1} , with a clear trend of decreasing for late B-types. In order to test the importance of neglecting macroturbulence in the synthetic FWHM of the He lines, we did a test calculation including a Gaussian macroturbulent velocity of 20 km s^{-1} . The results indicate that considering the uncertainties of the method adopted here, including macroturbulence at this level, has negligible effect in the measured FWHM of the synthetic spectra of sample He I lines.

The measured values of FWHM for the three He I lines used in the $v \sin i$ determinations are found in Table 2 (Columns 6–8); Columns 9–11 list the $v \sin i$ for each He line; Columns 12 and 13, the final $v \sin i$ values for the studied stars: these represent the average values and the standard deviations in each case. We note that $v \sin i$ were not derived for six stars with T_{eff} values higher than 33,700 K, as they fell out of the validity of the $v \sin i$ calibration from Daflon et al. (2007).

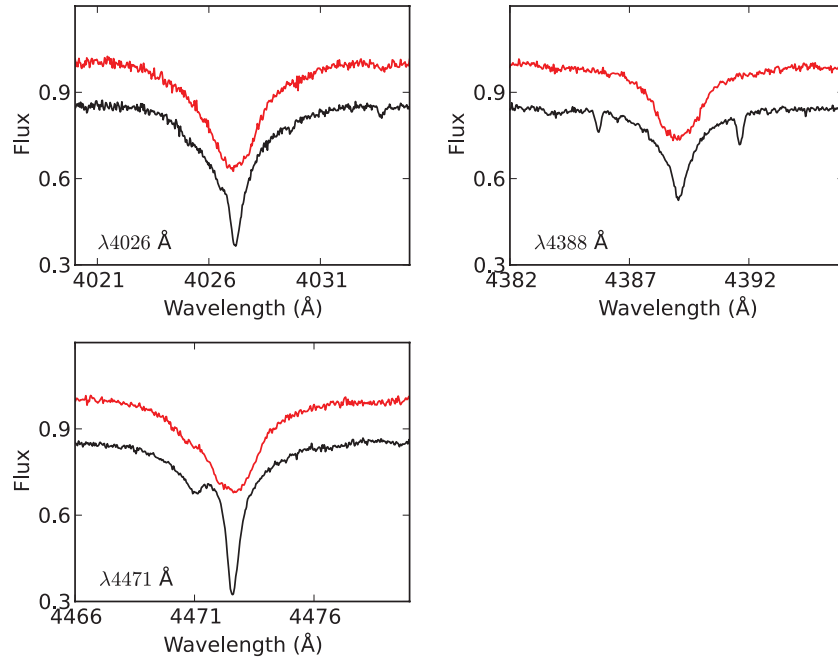


Figure 4. Sample spectra showing the three He I lines that were used to derive the projected rotational velocities for the target stars. The bottom spectra (black) in the three panels are for the star HIP 73624 with $v \sin i = 17 \text{ km s}^{-1}$ and the top spectra (red) are for the star HIP 33492 with $v \sin i = 71 \text{ km s}^{-1}$. The spectra were arbitrarily displaced in intensity for better viewing.

(A color version of this figure is available in the online journal.)

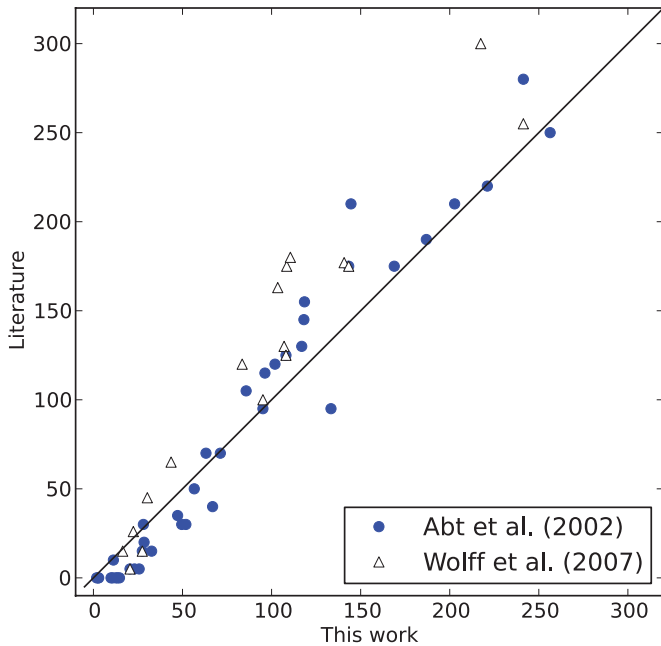


Figure 5. Comparison between the $v \sin i$ derived in this study for stars in common with other two studies in the literature: Abt et al. (2002) (blue circles) and Wolff et al. (2007) (white triangles). The solid line represents the locus of equal values.

(A color version of this figure is available in the online journal.)

Figure 5 shows a comparison of the $v \sin i$ results in this study with those from other determinations in the literature: results from Abt et al. (2002) are represented as filled blue circles while results from the Wolff et al. (2007) study are represented as red filled triangles. Abt et al. (2002) derived $v \sin i$ for a sample of B stars of the Bright Star Catalogue with luminosity classes between I and V, using a calibration for FWHM of He I and Mg II

lines anchored on standard stars of Slettebak et al. (1975). Wolff et al. (2007) obtained a relationship between FWHM and $v \sin i$ based on results from He I lines of Huang & Gies (2006). We note that the $v \sin i$ for the stars in common with Abt et al. (2002) are systematically lower than the ones here in the range between ~ 0 and 90 km s^{-1} ($\langle \Delta v \sin i \rangle$ (this study–Abt et al.) = 9 km s^{-1} for 24 stars in common); higher than ours in the range between 90 and 150 km s^{-1} ($\langle \Delta v \sin i \rangle$ (this study–Abt et al.) ≥ -15); and in rough agreement for the largest $v \sin i$ (except for one star). The $v \sin i$ in Wolff et al. (2007) are mostly higher than ours, except for stars with the lowest $v \sin i$. The average $v \sin i$ difference (this study–Wolff et al.) is -26 km s^{-1} for 17 stars in common. Given the uncertainties in the determinations and the methods adopted, there is reasonable agreement between the three different studies.

5. DISCUSSION

5.1. The Entire Sample

We start our discussion by showing results for the derived effective temperatures for the stars. A histogram showing the distribution of effective temperatures for 272 OB stars is shown in Figure 6. The effective temperatures of the target sample peak around $17,000 \text{ K}$, with most stars being cooler than $28,000 \text{ K}$.

Figure 7 illustrates the box plots for the $v \sin i$ values for the studied stars in each corresponding spectral type. The box extends from the lower to upper quartile values of the data, with a line at the median and a small box as the mean. The whiskers extend from the box to show the range of the data. The crosses are the outliers. An inspection of this figure indicates that the mean $v \sin i$ for each spectral type bin is roughly consistent with a constant value across spectral type. The average $v \sin i$ value computed for the studied sample is 98 km s^{-1} . Huang & Gies (2006) also found a distribution of mean $v \sin i$ for cluster stars, which is basically flat over a similar spectral type

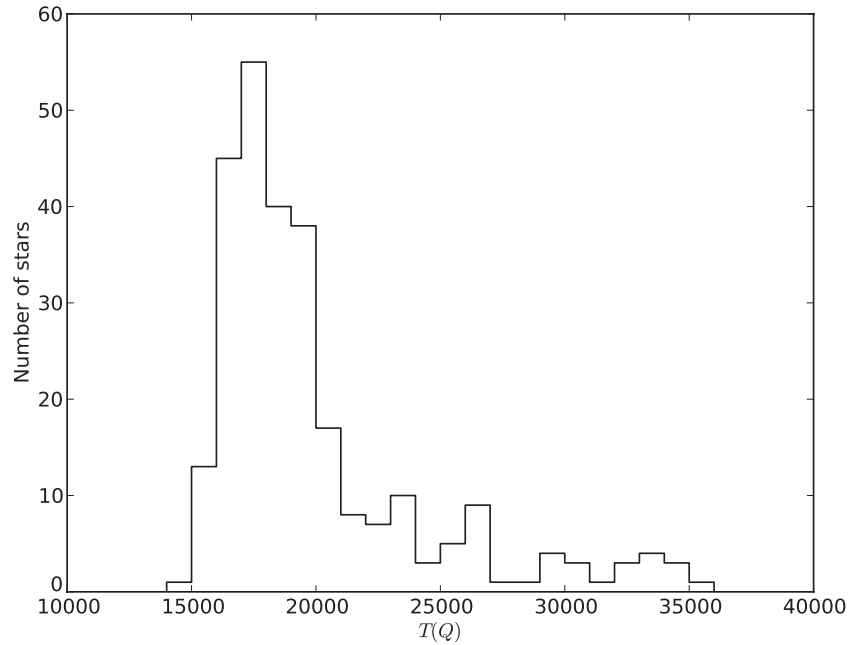


Figure 6. Histogram showing the distribution of effective temperatures for the studied sample.

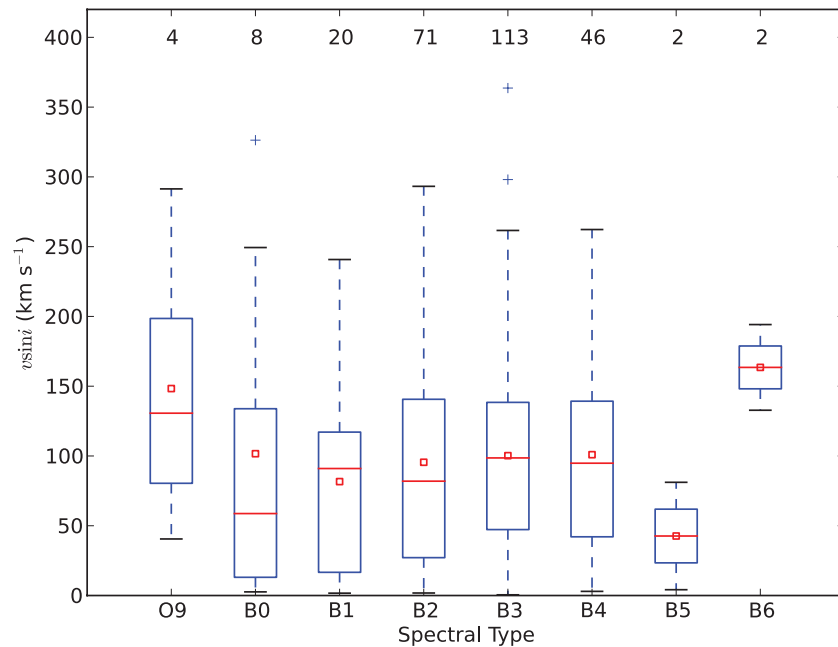


Figure 7. Box plot for the studied stars in terms of the spectral type. The average $v \sin i$ for the stars in each spectral type bin is roughly constant, even considering the least populated bins.

(A color version of this figure is available in the online journal.)

range, although their study also includes giant stars. Overall the mean $v \sin i$ obtained here for spectral type bins B0–B2 and B3–B5 are in rough agreement with the average results for luminosity classes IV and V in Abt et al. (2002) (see Section 4 for comparisons of the $v \sin i$ for stars in common in the two studies).

The $v \sin i$ distribution of the current sample of 266 O and B stars is shown in the top panel of Figure 8. The distribution has a modest peak at low $v \sin i$ (~ 0 – 50 km s^{-1}) but it is overall flat (a broad distribution) for $v \sin i$ roughly between 0 and 150 km s^{-1} ; the number of stars drops for higher values of $v \sin i$. As previously mentioned, the targets in this study were

selected considering only their spectral types in the *Hipparcos* catalog. The sample studied here includes both stars in clusters and OB associations, as well as isolated stars that can represent some sort of field population.

One of the difficulties in making meaningful comparisons between rotational velocity distributions of stars in clusters versus stars in the “field” is in defining what constitutes a “field” star sample. This discussion is, in fact, related to the question of whether OB stars can form in isolation and if all OB stars, although isolated, belonged in the past to a cluster. The initial idea was that OB stars were only formed in clusters and associations but later on were ejected or dispersed

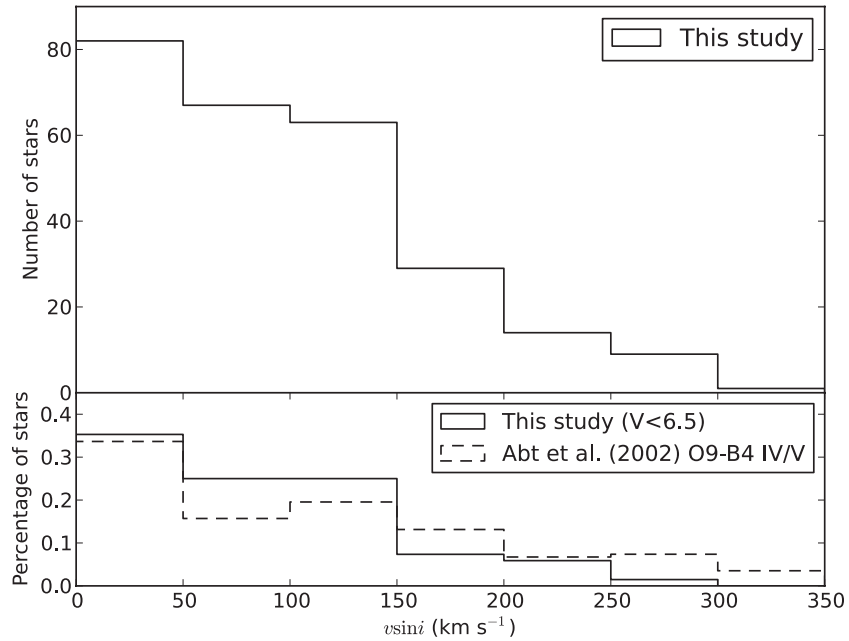


Figure 8. Histogram of $v \sin i$ distribution of our sample on the top panel. The bottom panel compares the normalized distribution of a subsample of stars in our sample with a magnitude cut in $V = 6.5$ and a sample with 312 field stars (spectral types O9–B4 IV/V) culled from Abt et al. (2002).

into the Galactic field. There is growing evidence, however, that at a least a small fraction of the O stars may be born in isolation (or from small molecular clouds). For instance, Krumholz et al. (2009) used a three-dimensional hydrodynamic simulation to show that the formation of isolated massive stars is possible; they successfully form a massive binary (having $41.5 M_{\odot}$ and $29.2 M_{\odot}$) from a $100 M_{\odot}$ molecular gas. One strong observational evidence that field OB stars may form in situ was presented by Lamb et al. (2010), who found very low mass companions around apparently isolated field OB stars in the Small Magellanic Cloud. Indeed, Oey & Lamb (2011) cite several lines of empirical evidence to suggest that in situ field massive stars constitute a significant, and perhaps dominant, component of the field OB star population.

Although samples of field stars are contaminated at some level with stars that are in the field now but were born in dense environments, a comparison of the $v \sin i$ obtained for the entire sample studied here with other samples taken as representative of the field population is of interest. Abt et al. (2002) provide the cornerstone work of the distributions of projected rotational velocities of the so-called field OB stars. The targets in that study were taken from the Bright Star Catalogue and also include stars that are members of clusters and associations. For the sake of comparison with a field sample that is representative of the spectral types and luminosity classes of most of the studied stars, we culled from the Abt et al. (2002) sample those stars with spectral types O9–B4 and luminosity classes IV and V. The distribution of $v \sin i$ for this subsample is shown as the dashed line histogram in the bottom panel of Figure 8. We thus selected those stars of our sample with $V < 6.5$, which is the magnitude limit of the Bright Star Catalogue (Hoffleit & Jaschek 1982) and this subsample is also presented in the bottom panel of Figure 8. A Kolmogorov–Smirnov (K-S) test gives more than 90% of probability that both distributions are drawn from the same population. These results suggest that the $v \sin i$ distribution obtained from Abt et al. (2002) for the so-called field population is similar from the $v \sin i$ distribution of our sample brighter stars.

5.2. Stars in OB Associations and Clusters

The idea that stellar rotation of OB stars in clusters relates to cluster density has been put forward in previous studies in the literature. In particular, comparisons between the $v \sin i$ distributions of stars from clusters, OB associations, or the field have shown that stellar members of dense associations or clusters rotate on average faster than member stars of unbound associations or the field (e.g., Wolff et al. 2007; Daflon et al. 2007). Previous studies discussing rotational velocity distributions of stars in clusters include Guthrie (1982), Wolff et al. (1982, 2007), Huang & Gies (2006, 2008), and Huang et al. (2010). In general, all these studies confirm that there seems to be real differences between the $v \sin i$ distributions of cluster members when compared to field; there are fewer slow rotators in the clusters when compared to the field or the stars in clusters tend to rotate faster. Guthrie (1982), however, found the presence of a bimodality in his $v \sin i$ distribution: the cluster distribution was double peaked with one at $v \sin i < 50 \text{ km s}^{-1}$ and the other at $v \sin i \sim 225 \text{ km s}^{-1}$.

A comparative study of the $v \sin i$ of all stars in our sample in connection with their birth environments (clusters/associations or field) is of interest but firmly establishing membership is a difficult task as detailed and careful membership determinations are beyond the scope of this paper. Instead, in this study, we use literature results in order to select a subsample of stars for which there is secure information on their membership. For OB associations, this is based on the list of probable members from the census of OB associations in the Galactic disk from the *Hipparcos* catalog by de Zeeuw et al. (1999) and in the study of the stellar content of the Orion association by Brown et al. (1994). In addition, we searched the target list in Humphreys & McElroy (1984) and found a few more targets to be association members. The stars in our sample members in higher density environments or clusters were obtained from cross checking the studied sample with the WEBDA open cluster database (Mermilliod & Paunzen 2003). In addition, we searched the open cluster member list of Robichon et al. (1999). The membership information for each star can be found in Column 15 of Table 2.

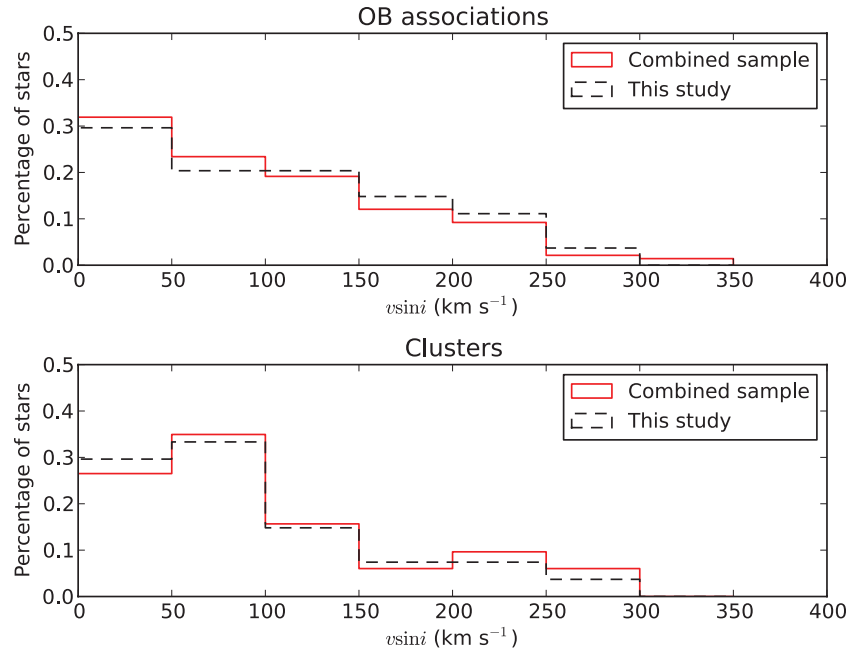


Figure 9. Distribution of $v \sin i$ for the studied samples of OB association (top panel) and cluster members (lower panel) are shown as red dashed line histograms. The black solid line histograms represent the combined sample: stars in this study plus 143 star members of clusters and associations from Daflon et al. (2007). Both studies use the same methodology to derive $v \sin i$.

(A color version of this figure is available in the online journal.)

Histograms showing the $v \sin i$ distributions for the culled subsamples of OB association and cluster members are shown in Figure 9 (red dashed line histograms). The black solid histograms represent a larger sample combining our sample with the sample of O and B stars from Daflon et al. (2007). In that paper, 143 OB star members of open cluster, OB associations, and 23 stars in H II regions have been observed in order to probe the radial metallicity gradient in Galactic disk. Since the $v \sin i$ in the present study were derived using the same grid and methodology as in Daflon et al. (2007), the discussion beyond this point will be based on the combined sample (black solid histograms) given better statistics. The distribution of $v \sin i$ obtained for the stars in OB associations (top panel) has a relatively larger number of objects with $v \sin i$ between 0 and 50 km s⁻¹ and the number of stars declines smoothly with $v \sin i$. For stars in clusters (bottom panel) there is a smaller fraction of slow rotating stars and an apparent peak at 50–100 km s⁻¹. The smooth distribution of $v \sin i$ values for the association members may result from a nearly single values for equatorial rotational velocity that is viewed at random inclination, while the cluster distribution may be more complex.

Figure 10 shows a comparison of the cumulative fractions for the $v \sin i$ distributions for the clusters and OB associations, as well as the field (from the subsample selected here from Abt et al. (2002) as discussed above). The field sample has a higher fraction of slowly rotating stars ($v \sin i$ between 0 and 50 km s⁻¹) when compared to the OB associations or clusters. In addition, there is a clear excess of stars with $v \sin i$ between roughly 70 and 130 km s⁻¹ in the cluster distribution when compared to the OB associations as well as the field. In fact, there seems to be a gradation from cluster to OB association to field confirming the trend found by Wolff et al. (2007). A K-S test between the field star sample and the association sample gives 92% probability that both samples are drawn from distinct populations and 88% probability that the cluster and the field are drawn from distinct populations. A K-S test between the OB associations and the

cluster distributions, however, gives only a 50% probability that these are drawn from distinct populations. Thus, any differences between the distributions of clusters and associations in this study are not so clear and may not be statistically significant; larger studies are needed.

5.3. Runaway Stars

Few studies in the literature have investigated the distribution of rotational velocities in runaway OB stars. Martin (2006) studied the properties of a population of stars far from the Galactic plane and this included a sample of 21 Population I runaway stars. The $v \sin i$ distribution for the runaway stars was found in that study to be broad with no apparent peaks in the range $v \sin i = 50$ to 200 km s⁻¹ and with a slight decline for values of $v \sin i$ below 50 km s⁻¹ (see Martin 2006, Figure 9(b)). The interpretation was that the projected rotational velocity distribution for the runaways was more similar to that of an OB association than to the field; one of the main distinctions when comparing with the field is the absence of a larger number of slow rotators in the distribution of the runaway sample.

Runaway stars can be explained by two scenarios: the binary supernova scenario, in which a star is ejected from the binary system when its companion turns into a supernova, and the dynamical ejection scenario, in which a star is ejected from its parent cluster or association due to dynamical processes. These objects are usually identified via one of three methods: spatial velocities, tangential velocities, or radial velocities. Tetzlaff et al. (2011) combined these three methods to identify runaway stars in the *Hipparcos* catalog. Our study has 34 stars identified as runaways in Tetzlaff et al.’s catalog of runaway candidates.

The $v \sin i$ distribution obtained for the runaway stars in our sample is shown as a solid line histogram in Figure 11. Two peaks are evident from a visual inspection of our distribution: one corresponding to slow rotating stars (or $v \sin i \sim$

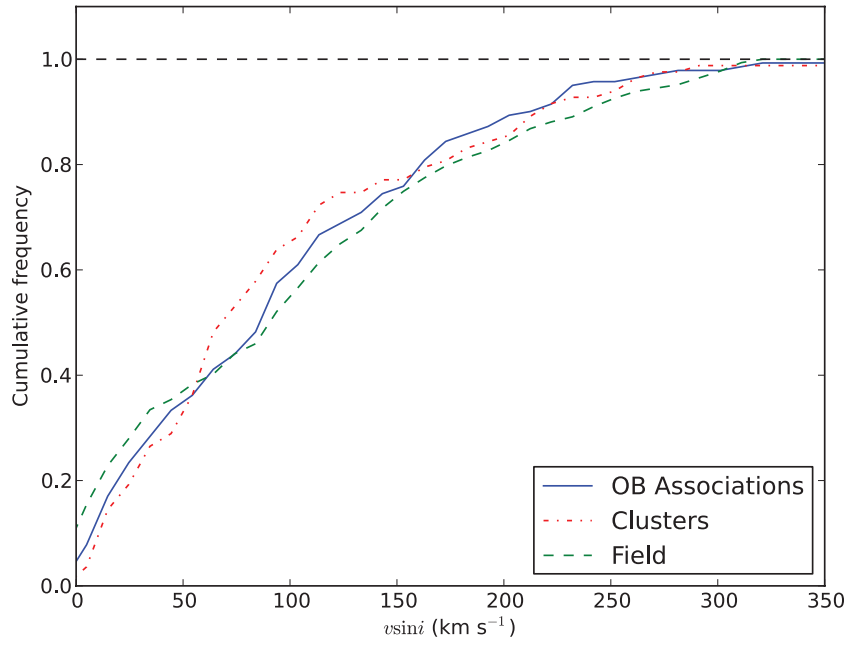


Figure 10. Cumulative fractions for the $v \sin i$ distributions for the clusters, OB associations, and the field. There seems to be a gradation from cluster to OB association to field. A K-S test between the field star sample and the association sample gives 92% probability that both samples are drawn from distinct populations and 88% probability that the cluster and the field are drawn from distinct populations. A K-S test between the OB associations and the cluster distributions, however, gives only a 50% probability that these are drawn from distinct populations.

(A color version of this figure is available in the online journal.)

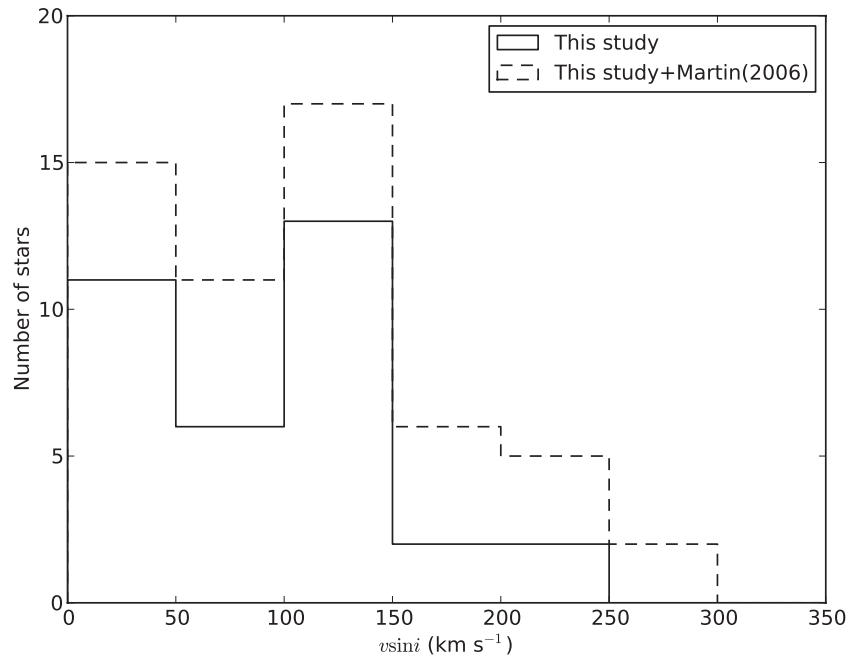


Figure 11. $v \sin i$ distribution for the runaway stars in our sample is shown (solid line histogram). The distribution has two peaks. A K-S test indicates that the runaway $v \sin i$ distribution is more similar to the cluster distribution. This could be an indication that the runaway stars originated from a dynamical ejection scenario. The presence of a second peak at low $v \sin i$ could be related to runaways ejected from OB associations. A histogram representing the combined sample including the runaway stars studied by Martin (2006) is also presented for comparison (dashed line histogram).

0–50 km s⁻¹) and another corresponding to higher projected rotational velocities ($v \sin i$ between 100 and 150 km s⁻¹). We also show for comparison a histogram representing the combined sample including the runaway stars studied by Martin (2006). Given that the distribution of $v \sin i$ in Martin (2006) runaway sample is generally flat, the two $v \sin i$ peaks observed in the solid line histogram remain in the combined sample.

A K-S test was run on the runaway $v \sin i$ distribution obtained in this study compared to the other three samples discussed previously: the field, the OB association, and the cluster subsamples. The probabilities that both distributions are drawn from the same populations are 18%, 40%, and 71%, respectively, for the field, association, and cluster. This is an indication that the runaway phenomenon maybe more likely

associated with the dense cluster environments, as expected from a dynamical ejection scenario. However, we note the lack of very massive and dense clusters nearby the Sun, which are the main sources of runaways ejected by means of the dynamical ejection scenario. As a final note, the presence of a second peak at low $v \sin i$ (~ 0 – 50 km s^{-1}) in the runaway distribution in this study could be related to runaways originating from OB associations. As discussed previously, stars in associations have typically lower $v \sin i$ when compared to cluster stars.

6. CONCLUSIONS

High-resolution spectroscopic observations and a first characterization of a sample of 350 OB stars have been carried out. Projected rotational velocities were obtained for 266 stars (after rejecting spectroscopic binaries/multiple systems) using measurements of FWHM of He I lines and interpolation in a synthetic grid from Daflon et al. (2007). The $v \sin i$ distribution obtained for the studied sample has a modest peak at low $v \sin i$ (~ 0 – 50 km s^{-1}) but it is overall flat for $v \sin i$ roughly between 0 and 150 km s^{-1} ; the number of stars drops for higher values of $v \sin i$. The $v \sin i$ distribution of our brighter sample stars is similar to the one obtained from a sample of field stars picked from the work of Abt et al. (2002).

Literature results on membership were used in order to identify subsamples of stars belonging to OB associations or clusters. We compared these two groups and found that star members of OB associations and clusters compose two distinct populations. The cluster stars tend to have higher $v \sin i$ when compared to the OB association subsample, which could mean that the stellar rotation of a population is dictated by the density of the cloud in which it forms. Also, when the OB association and cluster populations are compared with the field sample, it is found that the latter has a larger fraction of slowest rotators, as previously shown by other works. In fact, there seems to be a gradation from cluster to OB association to field in $v \sin i$ distribution.

The present sample has 34 stars that were identified as runaway candidates in Tetzlaff et al. (2011) catalog. The $v \sin i$ distribution of the runaway sample presents two peaks: one for $v \sin i \sim 0$ – 50 km s^{-1} and another for $v \sin i \sim 100$ – 150 km s^{-1} . The K-S test run with the runaway stars, OB association, cluster, and field samples indicates that the runaway $v \sin i$ distribution is more likely to be similar with the distribution of the denser environments, which could suggest that these stars were ejected through the dynamic ejection mechanism. Also, there is a possibility that the low $v \sin i$ peak is composed of stars that were ejected from OB associations.

We thank the referee for the careful reading and suggestions. We warmly thank Marcelo Borges, Catherine Garmany, John Glaspey, and Joel Lamb for fruitful discussion and comments on the manuscript. G.A.B. thanks the hospitality of University of Michigan on his visit and acknowledges Conselho Nacional de

Desenvolvimento Científico e Tecnológico (CNPq-Brazil) and Coordenação de Aperfeiçoamento de Pessoal de Nível Superior (CAPES - Brazil) for his fellowship. T.B. was funded by grant No. 621-2009-3911 from the Swedish Research Council (VR). M.S.O. and T.B. were supported in part by NSF-AST0448900. M.S.O. warmly thanks NOAO for the hospitality of a sabbatical visit. K.C. acknowledges funding from NSF grant AST-907873. This research has made use of the SIMBAD database, operated at CDS, Strasbourg, France.

Facility: Magellan:Clay

REFERENCES

- Abt, H. A., Levato, H., & Grosso, M. 2002, *ApJ*, **573**, 359
- Bernstein, R., Shectman, S. A., Gunnels, S. M., Mochnacki, S., & Athey, A. E. 2003, *Proc. SPIE*, **4841**, 1694
- Brown, A. G. A., de Geus, E. J., & de Zeeuw, P. T. 1994, *A&A*, **289**, 101
- Butler, K., & Giddings, J. R. 1985, *Newsletter Analysis Astron. Spectra*, **9**, 7
- Code, A. D., Bless, R. C., Davis, J., & Brown, R. H. 1976, *ApJ*, **203**, 417
- Daflon, S., Cunha, K., & Becker, S. R. 1999, *ApJ*, **522**, 950
- Daflon, S., Cunha, K., de Araújo, F. S. W., & Przybilla, N. 2007, *AJ*, **134**, 1570
- de Zeeuw, P. T., Hoogerwerf, R., de Bruijne, J. H. J., Brown, A. G. A., & Blaauw, A. 1999, *AJ*, **117**, 354
- Eggleton, P. P., & Tokovinin, A. A. 2008, *MNRAS*, **389**, 869
- Fitzgerald, M. P. 1970, *A&A*, **4**, 234
- Giddings, J. R. 1981, PhD thesis, Univ. London
- Guthrie, B. N. G. 1982, *MNRAS*, **198**, 795
- Harmanec, P., & Božić, H. 2001, *A&A*, **369**, 1140
- Hauck, B., & Mermilliod, M. 1980, *A&AS*, **40**, 1
- Hauck, B., & Mermilliod, M. 1998, *A&AS*, **129**, 431
- Hoffleit, D., & Jaschek, C. 1982, *The Bright Star Catalogue* (4th rev. ed.; New Haven: Yale Univ. Obs.)
- Huang, W., & Gies, D. R. 2006, *AJ*, **648**, 580
- Huang, W., & Gies, D. R. 2008, *AJ*, **683**, 1045
- Huang, W., Gies, D. R., & McSwain, M. V. 2010, *ApJ*, **722**, 605
- Hubeny, I. 1988, *Comput. Phys. Commun.*, **52**, 103
- Hubeny, I., & Lanz, T. 1995, *ApJ*, **439**, 875
- Humphreys, R. M., & McElroy, D. B. 1984, *ApJ*, **284**, 565
- Johnson, H. L. 1958, *Lowell Obs. Bull.*, **4**, 37
- Krumholz, M. R., Klein, R. I., McKee, C. F., Offner, S. S. R., & Cunningham, A. J. 2009, *Science*, **323**, 754
- Lamb, J. B., Oey, M. S., Werk, J. K., & Ingleby, L. D. 2010, *ApJ*, **725**, 1886
- Lefèvre, L., Marchenko, S. V., Moffat, A. F. J., & Acker, A. 2009, *A&A*, **507**, 1141
- Martin, J. C. 2006, *AJ*, **131**, 3047
- Massey, P., Silkey, M., Garmany, C. D., & Degioia-Eastwood, K. 1989, *AJ*, **97**, 107
- Mermilliod, J. 1987, *A&AS*, **71**, 413
- Mermilliod, J.-C., & Paunzen, E. 2003, *A&A*, **410**, 511
- Oey, M. S., & Lamb, J. B. 2011, arXiv:1109.07590
- Oudmaijer, R. D., & Parr, A. M. 2010, *MNRAS*, **405**, 2439
- Paunzen, E., Schnell, A., & Maitzen, H. M. 2005, *A&A*, **444**, 941
- Perryman, M. A. C., Lindegren, L., Kovalevsky, J., et al. 1997, *A&A*, **323**, 49
- Przybilla, N. 2005, *A&A*, **443**, 293
- Robichon, N., Arenou, F., Mermilliod, J.-C., & Turon, C. 1999, *A&A*, **345**, 471
- Simón-Díaz, S., Herrero, A., Uytterhoeven, K., et al. 2010, *ApJ*, **720**, 174
- Slettebak, A., Collins, G. W., II, Parkinson, T. D., Boyce, P. B., & White, N. M. 1975, *ApJS*, **29**, 137
- Tetzlaff, N., Neuhäuser, R., & Hohle, M. M. 2011, *MNRAS*, **410**, 190
- Walborn, N. R., & Fitzpatrick, E. L. 1990, *PASP*, **102**, 379
- Wolff, S. C., Edwards, S., & Preston, G. W. 1982, *ApJ*, **252**, 322
- Wolff, S. C., Strom, S. E., Dror, D., & Venn, K. 2007, *AJ*, **133**, 1092